

Measurement of the cosmic-ray proton spectrum from 40 GeV to 100 TeV with the DAMPE satellite

DAMPE Collaboration*: Q. An^{1,2}, R. Asfandiyarov³, P. Azzarello³, P. Bernardini^{4,5}, X. J. Bi^{6,7}, M. S. Cai^{8,9}, J. Chang^{8,9}, D. Y. Chen^{7,8}, H. F. Chen^{1,2†}, J. L. Chen¹⁰, W. Chen^{7,8}, M. Y. Cui⁸, T. S. Cui¹¹, H. T. Dai^{1,2}, A. D'Amone^{4,5}, A. De Benedittis^{4,5}, I. De Mitri^{12,13}, M. Di Santo^{4,5}, M. Ding^{7,10}, T. K. Dong⁸, Y. F. Dong⁶, Z. X. Dong¹¹, G. Donvito¹⁴, D. Droz³, J. L. Duan¹⁰, K. K. Duan^{7,8}, D. D'Urso^{15‡}, R. R. Fan⁶, Y. Z. Fan^{8,9}, F. Fang¹⁰, C. Q. Feng^{1,2}, L. Feng⁸, P. Fusco^{14,16}, V. Gallo³, F. J. Gan^{1,2}, M. Gao⁶, F. Gargano¹⁴, K. Gong⁶, Y. Z. Gong⁸, D. Y. Guo⁶, J. H. Guo^{8,9}, X. L. Guo^{8,9}, S. X. Han¹¹, Y. M. Hu⁸, G. S. Huang^{1,2}, X. Y. Huang⁸, Y. Y. Huang⁸, M. Ionica¹⁵, W. Jiang^{8,9}, X. Jin^{1,2}, J. Kong¹⁰, S. J. Lei⁸, S. Li^{7,8}, W. L. Li¹¹, X. Li⁸, X. Q. Li¹¹, Y. Li¹⁰, Y. F. Liang⁸, Y. M. Liang¹¹, N. H. Liao⁸, C. M. Liu^{1,2}, H. Liu⁸, J. Liu¹⁰, S. B. Liu^{1,2}, W. Q. Liu¹⁰, Y. Liu⁸, F. Loparco^{14,16}, C. N. Luo^{8,9}, M. Ma¹¹, P. X. Ma^{8,9}, S. Y. Ma^{1,2}, T. Ma⁸, X. Y. Ma¹¹, G. Marsella^{4,5}, M. N. Mazziotta¹⁴, D. Mo¹⁰, X. Y. Niu¹⁰, X. Pan^{8,9}, W. X. Peng⁶, X. Y. Peng⁸, R. Qiao⁶, J. N. Rao¹¹, M. M. Salinas³, G. Z. Shang¹¹, W. H. Shen¹¹, Z. Q. Shen^{7,8}, Z. T. Shen^{1,2}, J. X. Song¹¹, H. Su¹⁰, M. Su^{8,17}, Z. Y. Sun¹⁰, A. Surdo⁵, X. J. Teng¹¹, A. Tykhonov³, S. Vitillo³, C. Wang^{1,2}, H. Wang¹¹, H. Y. Wang^{6†}, J. Z. Wang⁶, L. G. Wang¹¹, Q. Wang^{1,2}, S. Wang^{7,8}, X. H. Wang¹⁰, X. L. Wang^{1,2}, Y. F. Wang^{1,2}, Y. P. Wang^{7,8}, Y. Z. Wang^{7,8}, Z. M. Wang^{12,13}, D. M. Wei^{8,9}, J. J. Wei⁸, Y. F. Wei^{1,2}, S. C. Wen^{1,2}, D. Wu⁶, J. Wu^{8,9}, L. B. Wu^{1,2}, S. S. Wu¹¹, X. Wu³, K. Xi¹⁰, Z. Q. Xia^{8,9}, H. T. Xu¹¹, Z. H. Xu^{8,9}, Z. L. Xu⁸, Z. Z. Xu^{1,2}, G. F. Xue¹¹, H. B. Yang¹⁰, P. Yang¹⁰, Y. Q. Yang¹⁰, Z. L. Yang¹⁰, H. J. Yao¹⁰, Y. H. Yu¹⁰, Q. Yuan^{8,9}, C. Yue^{7,8}, J. J. Zang⁸, F. Zhang⁶, J. Y. Zhang⁶, J. Z. Zhang¹⁰, P. F. Zhang⁸, S. X. Zhang¹⁰, W. Z. Zhang¹¹, Y. Zhang^{7,8}, Y. J. Zhang¹⁰, Y. L. Zhang^{1,2}, Y. P. Zhang¹⁰, Y. Q. Zhang^{7,8}, Z. Zhang⁸, Z. Y. Zhang^{1,2}, H. Zhao⁶, H. Y. Zhao¹⁰, X. F. Zhao¹¹, C. Y. Zhou¹¹, Y. Zhou¹⁰, X. Zhu^{1,2}, Y. Zhu¹¹, and S. Zimmer³

¹State Key Laboratory of Particle Detection and Electronics, University of Science and Technology of China, Hefei 230026, China

²Department of Modern Physics, University of Science and Technology of China, Hefei 230026, China

³Department of Nuclear and Particle Physics, University of Geneva, CH-1211, Switzerland

⁴Dipartimento di Matematica e Fisica E. De Giorgi, Università del Salento, I-73100, Lecce, Italy

⁵Istituto Nazionale di Fisica Nucleare (INFN) - Sezione di Lecce, I-73100, Lecce, Italy

*The correspondence should be addressed to: dampe@pmo.ac.cn

†Deceased.

‡Now at Università di Sassari, Dipartimento di Chimica e Farmacia, I-07100, Sassari, Italy

⁶Institute of High Energy Physics, Chinese Academy of Sciences, Yuquan Road 19B, Beijing 100049, China

⁷University of Chinese Academy of Sciences, Yuquan Road 19A, Beijing 100049, China

⁸Key Laboratory of Dark Matter and Space Astronomy, Purple Mountain Observatory, Chinese Academy of Sciences, Nanjing 210034, China

⁹School of Astronomy and Space Science, University of Science and Technology of China, Hefei 230026, China

¹⁰Institute of Modern Physics, Chinese Academy of Sciences, Nanchang Road 509, Lanzhou 730000, China

¹¹National Space Science Center, Chinese Academy of Sciences, Nanertiao 1, Zhongguancun, Haidian district, Beijing 100190, China

¹²Gran Sasso Science Institute (GSSI), Via Iacobucci 2, I-67100 L'Aquila, Italy

¹³Istituto Nazionale di Fisica Nucleare (INFN) -Laboratori Nazionali del Gran Sasso, I-67100 Assergi, L'Aquila, Italy

¹⁴Istituto Nazionale di Fisica Nucleare (INFN) - Sezione di Bari, I-70125, Bari, Italy

¹⁵Istituto Nazionale di Fisica Nucleare (INFN) - Sezione di Perugia, I-06123 Perugia, Italy

¹⁶Dipartimento di Fisica "M. Merlin" dell'Università e del Politecnico di Bari, I-70126, Bari, Italy

¹⁷Department of Physics and Laboratory for Space Research, the University of Hong Kong, Pok Fu Lam, Hong Kong, China

The precise measurement of the spectrum of protons, the most abundant component of the cosmic radiation, is necessary to understand the source and acceleration of cosmic rays in the Milky Way. This work reports the measurement of the cosmic ray proton fluxes with kinetic energies from 40 GeV to 100 TeV, with two and a half years of data recorded by the DArk Matter Particle Explorer (DAMPE). This is the first time an experiment directly measures the cosmic ray protons up to ~ 100 TeV with a high statistics. The measured spectrum confirms the spectral hardening found by previous experiments and reveals a softening at ~ 13.6 TeV, with the spectral index changing from ~ 2.60 to ~ 2.85 . Our result suggests the existence of a new spectral feature of cosmic rays at energies lower than the so-called knee, and sheds new light on the origin of Galactic cosmic rays.

Introduction

It is widely believed that the remnants of explosive stars in the Milky Way may play a substantial role in producing energetic cosmic ray (CR) particles (1, 2). The energy spectra of CRs are expected to be single power-laws (PLs) until the energies exceed the maximum acceleration limits of the sources, based on the conventional Fermi acceleration models (3). The diffusive transportation of CRs in the interstellar turbulent magnetic field results in a softening of the accelerated spectrum, by again a power-law form (for rigidities above a few tens of GV) according to the Boron-to-Carbon ratio (4). This general picture of CR production and propagation has been supported by measurements of CR energy spectra and composition ratios, as well as diffuse γ -rays (5).

However, such a simple picture has been challenged by some recent high-precision measurements. Remarkable spectral hardenings of the energy spectra of CRs were revealed in the ATIC (6, 7), CREAM (8, 9), PAMELA (10), and AMS-02 (11) observations. The spectral hardenings suggest extensions of the traditional CR source injection, acceleration, and/or propagation processes, e.g., refs. (12–14). The

spectral behaviors of CRs at higher energies ($> \text{TeV}$) are essential to understand the nature of the spectral hardenings, as well as the origin and propagation of CRs. Moreover, the extension of the spectra to PeV energies according to the power-law indices measured at sub-TeV energies seems to be in conflict with the all-particle spectrum of CRs (15). Such a puzzle may be solved if a significant spectral softening presents well below the so-called knee at several PeV. The precise measurements of the energy spectra of CRs above TeV are thus motivated by the test of potential new spectral features. Interestingly, the recent CREAM and NUCLEON data show hints that the energy spectra of CR nuclei may become softer above rigidities of $10 \sim 20 \text{ TV}$ (16, 17). However, the result of the proton plus helium spectrum from the air shower experiment ARGO-YBJ shows a single power-law form for energies between 3 and 300 TeV (18). The CREAM result is mainly limited by its low statistics. The NUCLEON data, with again a relatively low statistics at energies above tens TeV, also suffer from sizeable systematic uncertainties that need to be properly included. The indirect measurements, on the other hand, suffer from poor composition resolution. Although the magnetic spectrometers can measure CRs very accurately, they are unable to reach energies well beyond TeV in the foreseeable future. Therefore, the calorimeter-based direct measurement experiments, with high statistics up to $\sim 100 \text{ TeV}$ and well-controlled systematic uncertainties, are most suitable to solve the above problems.

Results

In this work we present the measurement of the proton spectrum with the Dark Matter Particle Explorer (DAMPE; also known as “Wukong” in China). DAMPE is a calorimetric-type, satellite-borne detector for observations of high energy electrons, γ -rays, and CRs (19, 20). From top to bottom, the instrument consists of a Plastic Scintillator strip Detector (PSD (21)), a Silicon-Tungsten tracker-converter (STK (22)), a bismuth germanate BGO imaging calorimeter (23), and a Neutron Detector (NUD (24)). The PSD measures the charge of incident particles, and serves as an anti-coincidence detector for γ -rays. The STK reconstructs the trajectory and also measures the charge of the particles. The BGO calorimeter

measures the energy and trajectory of incident particles, and provides effective electron/hadron discrimination based on the shower images. The NUD provides additional electron/hadron discrimination. These four sub-detectors enable good measurements of the charge ($|Z|$) with a resolution (Gaussian standard deviation) of about $0.06e$ and $0.04e$ for the PSD (25) and the STK respectively, the arrival direction with an angular resolution of better than 0.5° above 5 GeV, the energy with a resolution of higher than 1.5% for > 10 GeV electrons/photons (26) and about 25% \sim 35% for protons up to 10 TeV (20), and the identification of incoming particles with a proton rejection capability of about 3×10^4 when keeping 90% of electrons (26). The DAMPE detector was launched into a 500-km Sun-synchronous orbit on December 17, 2015. The on-orbit calibration results demonstrate that DAMPE operates stably in space (27).

The data used in this work cover the first 30 months of operation of DAMPE, from January 1, 2016 to June 30, 2018. The fraction of live time is about 75.73% after excluding the time when the satellite passes the South Atlantic Anomaly region, the instrument dead time, the time for on-orbit calibration, and the period between September 9, 2017 and September 13, 2017 during which a big solar flare occurred and may have affected the baseline of the detector. Protons are selected using the charge measured by the PSD (see the Materials and Methods for details about the event selection). Figure 1 illustrates the reconstructed PSD charge spectra for low- Z nuclei for deposited energies of 447 – 562 GeV (left panel), 4.47 – 5.62 TeV (middle panel), and 20 – 63 TeV (right panel), together with the Monte Carlo (MC) simulations of protons and helium nuclei with GEANT v4.10.03 (28). Note that small corrections from the reconstructed charge to the true particle charge (25) have not been applied in this work. The proton and helium peaks are clearly separated in this plot. The contamination of the proton sample due to helium nuclei is found to be less than 1% for deposited energies below 10 TeV and about 5% around 50 TeV, as an effect of the energy-dependent charge selection (see the Materials and Methods). Given the excellent electron-proton discrimination capability of DAMPE (26), the contamination due to residual electrons is estimated to be about 0.05% in the whole energy range analyzed in this work.

The proton spectrum in the energy range from 40 GeV to 100 TeV is shown in Figure 2 and tabulated

in Table 1. Error bars represent the 1σ statistical uncertainties of the DAMPE measurements, and the shaded bands show the systematic uncertainties associated with the analysis procedure (inner band) and the total systematic uncertainties including those from the hadronic models (outer band). Previous measurements by space detectors PAMELA (10) and AMS-02 (11), and balloon-borne detectors ATIC-2 (7), CREAM (16), and NUCLEON (17) are overlaid for comparison. The DAMPE spectrum is consistent with those of PAMELA and AMS-02. At higher energies, our results are also consistent with that of CREAM, ATIC-2, and NUCLEON when the systematic uncertainties are taken into account.

Discussion

The features of the proton spectrum measured by DAMPE in the energy range from 40 GeV to 100 TeV give fundamental information about the origin and propagation of Galactic CRs. A spectral hardening at a few hundred GeV energies is shown in our data, in agreement with that of PAMELA (10) and AMS-02 (11). As discussed in several papers (Ref. (29) and references therein) the hardening can be due to either details of the acceleration mechanism, effects in the propagation in the Milky Way, or the contribution of a new population of CRs (e.g. a nearby source). Furthermore, the DAMPE measurement gives, for the first time, a strong evidence of a softening at about 10 TeV. It is worth reminding that a maximum of the large-scale anisotropy has been observed just at that energy (see e.g., Ref. (29, 30)). We fit the spectrum with energies between 1 TeV and 100 TeV with a single power-law model and a smoothly broken power-law model respectively, and find that the smoothly broken power-law model is favored at the 4.7σ confidence level compared with the single power-law one (see the Materials and Methods for details of the fit). For the smoothly broken power-law model fit, the break energy is $13.6_{-4.8}^{+4.1}$ TeV, the spectral index below the break energy is 2.60 ± 0.01 , and the change of the spectral index above the break energy is -0.25 ± 0.07 . Results recently published by CREAM (16) and NUCLEON (17) experiments also indicate a spectral softening at rigidities of ~ 10 TV. However, these results are limited by low statistics or the lack of careful studies of systematic uncertainties.

The spectral hardening and softening are not compatible with the paradigm of a unique power-law spectrum up to the all-particle knee at PeV energies, thus implying a deep revision of CR modeling in the Galaxy. For instance the 10 TeV softening might be due to the exhaustion of the contribution of a given CR population. Either a local source on top of a power-law background (31), or various types of sources (32) can be compatible with this scenario. It should be noted that, the spectral softening should not correspond to the knee of protons; otherwise the expected all-particle spectrum would under-shoot the observational data, either for mass-dependent or charge-dependent knees of various species (15). Therefore, the current DAMPE measurement of the proton spectrum, together with other measurements from the space and groundbased experiments, puts a severe constraint on the models of Galactic CRs.

Materials and Methods

MC simulations

Extensive MC simulations are carried out to estimate the selection efficiencies, background contaminations, as well as the energy response matrix of hadronic cascades in the detector (in particular, the BGO calorimeter). The GEANT v4.10.03 (28) is adopted for these simulations. There are two typical hadronic interaction models in the GEANT simulation tool, the QGSP_FTFP_BERT and FTFP_BERT models. Comparisons of the shower development (longitude and transverse distributions) between simulations and the beam-test and on-orbit data show that the FTFP_BERT model matches better with the data. Therefore we adopt the FTFP_BERT model as the benchmark one of the MC simulations for incident energies less than 100 TeV. For higher energies we employ the FLUKA tool which links the DPMJET model for the simulation (33). The FLUKA based results are also used as a cross check and an estimate of the systematic uncertainties of the hadronic interaction models through comparing with the GEANT results.

An isotropic flux with $E^{-1.0}$ spectrum is generated for the detector simulation. We simulated protons, helium nuclei, and electrons in this analysis. After the charge selection, heavier nuclei are negligible for

the proton analysis. In the analysis, the spectra are re-weighted to $E^{-2.7}$ for protons and helium nuclei, and to $E^{-3.15}$ for electrons. The final proton spectrum we measured is not exactly the same as $E^{-2.7}$. However, changing the re-weight spectrum with indices from 2.5 to 3.1 has little influence on the results.

Proton event selection

The events with energy deposit in the BGO calorimeter larger than 20 GeV are selected in this analysis in order to suppress the effect of the geomagnetic rigidity cutoff. The detailed event selection method is described as follows.

- Pre-selection

DAMPE has four different triggers implemented on orbit: the Unbiased trigger, the Minimum Ionizing Particle (MIP) trigger, the Low-Energy (LE) trigger, and the High-Energy (HE) trigger (20). The events are required to satisfy the HE trigger condition to guarantee that the shower development starts before or at the top of the calorimeter. We further require that there are one or more hits in each sub-layer of the PSD and at least one good track (defined below) in the STK.

To check the MC trigger efficiency with the flight data, the events with coincidence of signals from the first two BGO layers, tagged as unbiased triggers, are used. The unbiased trigger events are pre-scaled by 1/512 at low latitudes ($\leq 20^\circ$) and 1/2048 at high latitudes. The HE trigger efficiency is estimated as $\varepsilon_{\text{trigger}} = \frac{N_{\text{HE|Unb}}}{N_{\text{Unb}}}$, where N_{Unb} is the number of events which pass the unbiased trigger condition and the proton selection (without the requirement of the HE trigger), and $N_{\text{HE|Unb}}$ is the number of events which further pass the HE trigger.

- Track selection

The track reconstruction algorithm may give more than one track due to the back-scattering particles. Here we define the “good” track as that the track has at least 4 hits in both the xz and yz layers, the reduced χ^2 value of the fit is smaller than 25, and the angular deviation from the BGO shower axis is within 5° . In the presence of multiple good tracks in the STK, we select the “best”

one through a combined assessment of the length of the track and the match between the candidate track and the shower axis in the calorimeter. Specifically, the selected tracks are required to be the longest among all the good tracks, among which the one closest to the shower axis is finally selected. We then apply the geometry cut on the selected track, which is required to pass through all the sub-layers of the PSD and the calorimeter from top to bottom.

To validate the STK track efficiency, we select a proton sample based on the BGO-reconstructed tracks. The track efficiency is estimated as the ratio of the number of events passing the above STK track selection to the total number of events.

- Charge selection

The ionization energy loss in the PSD is employed to measure the charge of the incoming particle. The charge is measured independently by the two PSD layers, which are averaged to get the final value. The measured charge is corrected for the path length of the particle in the PSD bars using the track information. The PSD and STK alignments are performed to maximally profit the charge reconstruction capabilities of the detector (34, 35). The charge measurements of the MC simulations show an energy-dependent difference from that of the flight data, due primarily to the back-scattering particles. To reduce the effect on the charge selection efficiency and the Helium background estimate, we apply energy-dependent corrections of the charge measurements for the MC simulations. We first parameterize the charge distributions of protons and helium nuclei in different deposited energy bins with a Landau-Gaussian convolution function, and fit the function to the flight data and MC data separately. Then the MC charges are shifted and shrunk according to the best-fitting parameters to match with the flight data. Proton candidates are selected through a cut of the PSD charge. This cut depends on the BGO deposited energy (E_{dep}) as

$$0.6 + 0.05 \cdot \log(E_{\text{dep}}/10 \text{ GeV}) \leq Z_{\text{PSD}} \leq 1.8 + 0.002 \cdot \log^4(E_{\text{dep}}/10 \text{ GeV}). \quad (1)$$

Note that this charge selection follows generally the logarithmic dependence of the ionization

energy loss in the PSD with particle energy. It enables us to have a very small contamination from Helium, i.e., less than 1% for deposited energies below 10 TeV and about 5% around 50 TeV. However, this selection results in an energy-dependent selection efficiency for protons, ranging from 94% for incident energies of 0.5 TeV to about 75% above 50 TeV. The charge selection efficiency for protons as a function of incident energy, derived from the GEANT4 FTFP_BERT MC simulations, is shown in Figure 3(a). This efficiency is used in deriving the effective acceptance shown in Figure 3(d).

The MC charge selection efficiency of each layer of the PSD is also validated by the flight data. For instance, to estimate the efficiency of the first PSD layer, we use the second PSD layer and the first STK layer measurements of the charge to select the sample, and calculate how many of the events have correct charge measurement in the first PSD layer. The differences between MC simulations and the flight data are adopted as systematic uncertainties of the charge selection efficiencies.

Background estimate

The background for protons includes mis-identified helium nuclei and a tiny fraction of electrons. The electrons are rejected thanks to different developments between hadronic showers and electromagnetic ones in the BGO calorimeter. The fraction of residual electrons in the proton sample is estimated to be about 0.05% for deposited energies larger than 20 GeV, using the template fit of the shower morphology parameter (ζ as defined in Ref. (26)). Helium nuclei are the main source of background for protons. We employ the template fit of the PSD charge spectra to estimate the helium backgrounds. The templates are built based on MC simulations (see Figure 1). The fraction of helium contamination as a function of deposited energy in the BGO calorimeter is shown in Figure 3(b). It is $\lesssim 1\%$ for deposited energies below 10 TeV, and increases up to $\sim 5\%$ around 50 TeV.

Energy measurement and spectral deconvolution

The energy of an incident particle is measured by the BGO calorimeter. Due to the limited thickness of the BGO calorimeter (~ 1.6 nuclear interaction length) and the missing energy due to muon and neutrino components in hadronic showers, the energy measurements of CR nuclei are biased with some uncertainties. Therefore MC simulations are required to estimate the energy response of the calorimeter. The energy resolution for protons is found to be about 25% \sim 35% for incident energies from 100 GeV to 10 TeV (20). The linear region of the energy measurement can extend to incident energies of ~ 100 TeV, thanks to the maximum reachable energy of 4 TeV for the dynode-2 readout device of each BGO bar (20). For very few highest energy events, the saturation of the maximum energy deposited BGO bar has been corrected based on the simulated transverse shower profile. The Engineering Qualification Model of DAMPE was extensively tested using test beams at the European Organization for Nuclear Research (CERN) in 2014-2015 (36, 37). The test beam momenta are 5, 10, 150, and 400 GeV/c, respectively. The comparison between the test beam data and MC simulations shows a good agreement with each other (20). The on-orbit calibration of the energy measurement is done by means of the MIP signals in each BGO crystal (27).

A deconvolution of the measured energy distribution into the incident energy distribution is applied. The number of events in the i -th deposited energy bin, $N_{\text{dep},i}$, can be obtained via the sum of number of events $N_{\text{inc},j}$ in all the incident energy bins weighted by the energy response matrix

$$N_{\text{dep},i} = \sum_j M_{ij} N_{\text{inc},j}, \quad (2)$$

where M_{ij} is the probability that an event in the j th incident energy bin is detected in the i -th deposited energy bin. We use MC simulations to derive the energy response matrix, applying the same selections as described above. Figure 3(c) shows the energy response matrix for different incident energies, for the FTFP_BERT model. The color represents the relative probability that a proton with E_{inc} deposits E_{dep} energy in the calorimeter. Eq. (2) is solved with a Bayesian method to derive the incident event

distribution (38).

Acceptance and absolute flux

The effective acceptance is defined as the product of the geometric factor and selection efficiencies (including energy, trigger, track, and charge selections). The effective acceptance for the i -th incident energy bin is calculated as

$$A_{\text{eff},i} = A_{\text{gen}} \times \frac{N_{\text{pass},i}}{N_{\text{gen},i}}, \quad (3)$$

where A_{gen} is the geometrical factor of the MC generation sphere, $N_{\text{gen},i}$ and $N_{\text{pass},i}$ are the numbers of generated events and those passing the selections. All efficiencies and the effective acceptance are obtained via the MC simulations. For the selection efficiencies, we have compared the MC simulations and the flight data with selected control samples (see the previous ‘‘Proton event selection’’ section), and the differences are adopted as an estimate of the systematic uncertainties of the effective acceptance. Figure 3(d) shows the effective acceptance as a function of incident energy.

The absolute proton flux F in the incident energy bin $[E_i, E_i + \Delta E_i]$ is then

$$F(E_i, E_i + \Delta E_i) = \frac{N_{\text{inc},i}}{\Delta E_i A_{\text{eff},i} T_{\text{exp}}}, \quad (4)$$

where ΔE_i is the width of the energy bin and T_{exp} is the exposure time.

Systematic uncertainties

Several types of systematic uncertainties are investigated in this analysis, including the event selection, the background subtraction, the spectral deconvolution procedure, and the energy response. The systematic uncertainties related with the event selection are estimated through comparisons between MC simulations and the flight data. The total uncertainty of the selection efficiencies is

$$\sigma_{\text{sel}} = \sqrt{\sigma_{\text{trigger}}^2 + \sigma_{\text{track}}^2 + \sigma_{\text{charge}}^2} \approx 4.7\%, \quad (5)$$

where $\sigma_{\text{trigger}} \approx 2.5\%$, $\sigma_{\text{track}} \approx 3.5\%$, and $\sigma_{\text{charge}} \approx 1.8\%$ are the corresponding systematic uncertainties of the trigger, track selection, and charge selection efficiencies.

The uncertainties due to the spectral deconvolution are estimated to be $\lesssim 1\%$, through re-generation of the response matrix and varying the spectral index from 2.5 to 3.1 when re-weighting the simulation data. The systematic uncertainties due to the Helium background subtraction are estimated through varying the charge selection condition Eq. (1) by $\pm 10\%$, and repeating the analysis. The background subtraction gives $\sim 0.1\%$ systematic uncertainties below 40 TeV and increases to $\sim 5\%$ at higher energies. The above systematic uncertainties are added in quadrature to give the total systematic uncertainties associated with the analysis procedure (σ_{ana} as given in Table 1).

The uncertainties of the fluxes due to different hadronic interaction models are estimated to be about 7% for energies less than 400 GeV via comparisons of the HE trigger efficiency and the energy deposit fraction between the 400 GeV test beam data and the GEANT FTFP_BERT simulation. Note that the 5 and 10 GeV test beam data are out of the interested energy range of the current study, and the 150 GeV test beam is limited by statistics and thus not used. For higher energies, we use the difference between the GEANT FTFP_BERT model and the FLUKA model to estimate such systematic uncertainties, which vary from 7% to 10%. A further check of the DPMJET model with the CRMC (39) interface gives negligible difference compared with the FLUKA model. Finally, the uncertainties associated with the absolute energy scale are about 2% (40), which are not corrected in this work.

Figure 4 summarizes the energy-dependent relative uncertainties of the proton fluxes. The statistical uncertainties refer to the Poisson fluctuations of the detected numbers of events in each deposited energy bin. To get the statistical uncertainties of the unfolded proton fluxes, an error propagation from the detected events to the unfolded fluxes is necessary in order to properly take into account the bin-by-bin migration due to the unfolding procedure (38). To obtain a proper estimate of the full error propagation, we run toy-MC simulations to generate fake observations in each deposited energy bin following the Poisson distribution, and get the proton fluxes through the unfolding procedure. The root-mean-squares of the resulting proton fluxes are taken as the 1σ statistical uncertainties. We find that the systematic uncertainties due to the hadronic interaction models dominate in the whole energy range. The STK track

efficiency uncertainties are the sub-dominant ones. In Table 1 the statistical uncertainties, the systematic one associated with the analysis procedure (added quadratically), and the systematic ones due to hadronic models are presented separately.

Comparison of different spectral models

To quantify the spectral behaviors of the proton spectrum, we use a power-law (PL) function

$$F(E) = F_0 \left(\frac{E}{\text{TeV}} \right)^{-\gamma} \quad (6)$$

or a smoothly broken power-law (SBPL) one

$$F(E) = F_0 \left(\frac{E}{\text{TeV}} \right)^{-\gamma} \left[1 + \left(\frac{E}{E_b} \right)^s \right]^{\Delta\gamma/s} \quad (7)$$

to fit the data.

We first focus on the high-energy part of the spectrum from 1 TeV to 100 TeV. To properly account for the systematic uncertainties, we adopt a set of independent nuisance parameters w_j , which are multiplied on the input model (41). The χ^2 function is defined as

$$\chi^2 = \sum_{i=8}^{17} \left[\frac{F(E_i)S(E_i; \mathbf{w}) - F_i}{\sigma_{\text{stat},i}} \right]^2 + \sum_{j=1}^m \left(\frac{1 - w_j}{\tilde{\sigma}_{\text{sys},j}} \right)^2, \quad (8)$$

where E_i , F_i and $\sigma_{\text{stat},i}$ are the median energy, flux and statistical uncertainty of the measurement in the i th energy bin, $F(E_i)$ is the model predicted flux in corresponding energy bin, $S(E_i; \mathbf{w})$ is a piecewise function defined by its value w_j in corresponding energy range covered by the j th nuisance parameter, and $\tilde{\sigma}_{\text{sys},j} = \sqrt{\sigma_{\text{ana}}^2 + \sigma_{\text{had}}^2}/F$ is the relative systematic uncertainty of the data in such an energy range. The last term in the right-hand-side is a Gaussian prior of the nuisance parameters. The energy range of [1, 100] TeV is logarithmically divided into m pieces. According to the energy-dependence of the systematic uncertainties in our work (Figure 5), we adopt $m = 4$ in the energy band of the fit which corresponds to 2 nuisance parameters per decade of energies.

The fit to the PL model gives $\chi^2/\text{dof} = 28.6/4$, where dof means the number of degree-of-freedom. For the SBPL model, we fix the smoothness parameter s to be 5.0 due to a lack of good constraint on

it, and get $\chi^2/\text{dof} = 2.5/2$. The results differ little for different values of s . The reduction of the χ^2 value is about 26.1 for two more free parameters, suggesting a significance of $\sim 4.7\sigma$ in favor of the SBPL model compared with the PL model. The fit of the SBPL model gives $F_0 = (8.68_{-0.45}^{+0.50}) \times 10^{-5} \text{ GeV}^{-1} \text{ m}^{-2} \text{ s}^{-1} \text{ sr}^{-1}$, $\gamma = 2.60 \pm 0.01$, $E_b = 13.6_{-4.8}^{+4.1} \text{ TeV}$, and $\Delta\gamma = -0.25 \pm 0.07$. The comparison of the best-fit result (solid line) with the data is shown in Figure 5. We also test the fitting with $m = 3$ (or 5), and find that the fitting parameters change very little, while the significance in favor of the SBPL model becomes 6.9σ (or 4.2σ).

We also fit the low energy part of the spectrum from 100 GeV to 6.3 TeV using the SBPL model to address the spectral hardening feature. Again 4 nuisance parameters are assumed, and s is fixed to be 5.0 which is close to that obtained by fitting the AMS-02 spectrum (11). The fitting model parameters are $F_0 = (7.58_{-0.31}^{+0.36}) \times 10^{-5} \text{ GeV}^{-1} \text{ m}^{-2} \text{ s}^{-1} \text{ sr}^{-1}$, $\gamma = 2.772 \pm 0.002$, $E_b = 0.48 \pm 0.01 \text{ TeV}$, $\Delta\gamma = 0.173 \pm 0.007$. As comparisons, the fit to the PAMELA data gives (10) $E_b = 0.232_{-0.030}^{+0.035} \text{ TeV}$, $\gamma = 2.850 \pm 0.016$, and $\Delta\gamma = 0.18 \pm 0.06$, and the fit to the AMS-02 spectrum gives (11) $E_b = 0.34_{-0.05}^{+0.09} \text{ TeV}$, $\gamma = 2.849_{-0.005}^{+0.006}$, and $\Delta\gamma = 0.133_{-0.037}^{+0.056}$, respectively. Our low-energy spectrum is slightly harder than that measured by PAMELA and AMS-02. The break energy inferred from the DAMPE data is roughly consistent with that of AMS-02, but is slightly higher than that of PAMELA. The $\Delta\gamma$ values of these three results are consistent with each other. Nevertheless, we should note that the fitting functions and energy ranges adopted in Refs. (10, 11) are not exactly the same as those in our work, and the comparison of the detailed numbers should be done with caution.

Note added: During the final stage for the publication of this paper, the CALET collaboration reported new measurements of the proton spectrum from 50 GeV to 10 TeV and confirmed the spectral hardening feature found by other measurements (42). The lack of measurements above 10 TeV of CALET, however, hampers a crosscheck of our main finding.

References and Notes

1. I. A. Grenier, J. H. Black, and A. W. Strong. The Nine Lives of Cosmic Rays in Galaxies. *Annu. Rev. Astron. Astrophys.*, 53:199–246, August 2015.
2. W. Baade and F. Zwicky. Remarks on Super-Novae and Cosmic Rays. *Physical Review*, 46:76–77, July 1934.
3. E. Fermi. On the Origin of the Cosmic Radiation. *Physical Review*, 75:1169–1174, April 1949.
4. M. Aguilar, L. Ali Cavazonza, G. Ambrosi, L. Arruda, N. Attig, S. Aupetit, P. Azzarello, A. Bachlechner, F. Barao, A. Barrau, L. Barrin, A. Bartoloni, L. Basara, S. Basegmez-du Pree, M. Battarbee, R. Battiston, U. Becker, M. Behlmann, B. Beischer, J. Berdugo, B. Bertucci, K. F. Bindel, V. Bindi, G. Boella, W. de Boer, K. Bollweg, V. Bonnivard, B. Borgia, M. J. Boschini, M. Bourquin, E. F. Bueno, J. Burger, F. Cadoux, X. D. Cai, M. Capell, S. Caroff, J. Casaus, G. Castellini, F. Cervelli, M. J. Chae, Y. H. Chang, A. I. Chen, G. M. Chen, H. S. Chen, L. Cheng, H. Y. Chou, E. Choumilov, V. Choutko, C. H. Chung, C. Clark, R. Clavero, G. Coignet, C. Consolandi, A. Contin, C. Corti, W. Creus, M. Crispoltoni, Z. Cui, Y. M. Dai, C. Delgado, S. Della Torre, O. Demakov, M. B. Demirkoz, L. Derome, S. Di Falco, F. Dimiccoli, C. Diaz, P. von Doetinchem, F. Dong, F. Donnini, M. Duranti, D. D’Urso, A. Egorov, A. Eline, T. Eronen, J. Feng, E. Fiandrini, E. Finch, P. Fisher, V. Formato, Y. Galaktionov, G. Gallucci, B. Garcia, R. J. Garcia-Lopez, C. Gargiulo, H. Gast, I. Gebauer, M. Gervasi, A. Ghelfi, F. Giovacchini, P. Goglov, D. M. Gomez-Coral, J. Gong, C. Goy, V. Grabski, D. Grandi, M. Graziani, K. H. Guo, S. Haino, K. C. Han, Z. H. He, M. Heil, J. Hoffman, T. H. Hsieh, H. Huang, Z. C. Huang, C. Huh, M. Incagli, M. Ionica, W. Y. Jang, H. Jinchi, S. C. Kang, K. Kanishev, G. N. Kim, K. S. Kim, Th. Kirn, C. Konak, O. Kounina, A. Kounine, V. Koutsenko, M. S. Krafczyk, G. La Vacca, E. Laudi, G. Laurenti, I. Lazzizzera, A. Lebedev, H. T. Lee, S. C. Lee, C. Leluc, H. S. Li, J. Q. Li, J. Q. Li, Q. Li, T. X. Li, W. Li, Y. Li, Z. H. Li, Z. Y. Li, S. Lim, C. H. Lin, P. Lipari, T. Lippert, D. Liu, Hu Liu, V. D. Lordello, S. Q. Lu, Y.

S. Lu, K. Luebelsmeyer, F. Luo, J. Z. Luo, S. S. Lv, F. Machate, R. Majka, C. Mana, J. Marin, T. Martin, G. Martinez, N. Masi, D. Maurin, A. Menchaca-Rocha, Q. Meng, V. M. Mikuni, D. C. Mo, L. Morescalchi, P. Mott, T. Nelson, J. Q. Ni, N. Nikonov, F. Nozzoli, A. Oliva, M. Orcinha, F. Palmonari, C. Palomares, M. Paniccia, M. Pauluzzi, S. Pensotti, R. Pereira, N. Picot-Clemente, F. Pilo, C. Pizzolotto, V. Plyaskin, M. Pohl, V. Poireau, A. Putze, L. Quadrani, X. M. Qi, X. Qin, Z. Y. Qu, T. Raiha, P. G. Rancoita, D. Rapin, J. S. Ricol, S. Rosier-Lees, A. Rozhkov, D. Rozza, R. Sagdeev, J. Sandweiss, P. Saouter, S. Schael, S. M. Schmidt, A. Schulz von Dratzig, G. Schwering, E. S. Seo, B. S. Shan, J. Y. Shi, T. Siedenburger, D. Son, J. W. Song, W. H. Sun, M. Tacconi, X. W. Tang, Z. C. Tang, L. Tao, D. Tescaro, Samuel C. Ting, S. M. Ting, N. Tomassetti, J. Torsti, C. Turkoglu, T. Urban, V. Vagelli, E. Valente, C. Vannini, E. Valtonen, M. Vazquez Acosta, M. Vecchi, M. Velasco, J. P. Vialle, V. Vitale, S. Vitillo, L. Q. Wang, N. H. Wang, Q. L. Wang, X. Wang, X. Q. Wang, Z. X. Wang, C. C. Wei, Z. L. Weng, K. Whitman, J. Wienkenhover, H. Wu, X. Wu, X. Xia, R. Q. Xiong, W. Xu, Q. Yan, J. Yang, M. Yang, Y. Yang, H. Yi, Y. J. Yu, Z. Q. Yu, S. Zeissler, C. Zhang, J. Zhang, J. H. Zhang, S. D. Zhang, S. W. Zhang, Z. Zhang, Z. M. Zheng, Z. Q. Zhu, H. L. Zhuang, V. Zhukov, A. Zichichi, N. Zimmermann, P. Zuccon. Precision Measurement of the Boron to Carbon Flux Ratio in Cosmic Rays from 1.9 GV to 2.6 TV with the Alpha Magnetic Spectrometer on the International Space Station. *Phys. Rev. Lett.*, 117(23):231102, December 2016.

5. A. W. Strong, I. V. Moskalenko, and V. S. Ptuskin. Cosmic-Ray Propagation and Interactions in the Galaxy. *Annual Review of Nuclear and Particle Science*, 57:285–327, November 2007.
6. J. P. Wefel, J. H. Adams, H. S. Ahn, G. L. Bashindzhagyan, K. Batkov, J. Chang, M. Christl, A. R. Fazely, O. Ganel, R. M. Gunasingha, T. G. Guzik, J. Isbert, K. C. Kim, E. N. Kouznetsov, M. I. Panasyuk, A. D. Panov, W. K. H. Schmidt, E. S. Seo, N. V. Sokolskaya, J. Wu, and V. I. Zatsepin. Energy Spectra of H and He from the ATIC-2 Experiment. *International Cosmic Ray Conference*,

3:105, 2005.

7. A. D. Panov, J. H. Adams, H. S. Ahn, G. L. Bashinzhagyan, J. W. Watts, J. P. Wefel, J. Wu, O. Ganel, T. G. Guzik, V. I. Zatsepin, I. Isbert, K. C. Kim, M. Christl, E. N. Kouznetsov, M. I. Panasyuk, E. S. Seo, N. V. Sokolskaya, J. Chang, W. K. H. Schmidt, and A. R. Fazely. Energy spectra of abundant nuclei of primary cosmic rays from the data of ATIC-2 experiment: Final results. *Bulletin of the Russian Academy of Sciences, Physics*, 73:564–567, June 2009.
8. H. S. Ahn, P. Allison, M. G. Bagliesi, L. Barbier, J. J. Beatty, G. Bigongiari, T. J. Brandt, J. T. Childers, N. B. Conklin, S. Coutu, M. A. Du Vernois, O. Ganel, J. H. Han, J. A. Jeon, K. C. Kim, M. H. Lee, P. Maestro, A. Malinine, P. S. Marrocchesi, S. Minnick, S. I. Mognet, S. W. Nam, S. Nutter, I. H. Park, N. H. Park, E. S. Seo, R. Sina, P. Walpole, J. Wu, J. Yang, Y. S. Yoon, R. Zei, and S. Y. Zinn. Energy Spectra of Cosmic-ray Nuclei at High Energies. *Astrophys. J.*, 707:593–603, December 2009.
9. H. S. Ahn, P. Allison, M. G. Bagliesi, J. J. Beatty, G. Bigongiari, J. T. Childers, N. B. Conklin, S. Coutu, M. A. DuVernois, O. Ganel, J. H. Han, J. A. Jeon, K. C. Kim, M. H. Lee, L. Lutz, P. Maestro, A. Malinin, P. S. Marrocchesi, S. Minnick, S. I. Mognet, J. Nam, S. Nam, S. L. Nutter, I. H. Park, N. H. Park, E. S. Seo, R. Sina, J. Wu, J. Yang, Y. S. Yoon, R. Zei, and S. Y. Zinn. Discrepant Hardening Observed in Cosmic-ray Elemental Spectra. *Astrophys. J. Lett.*, 714:L89–L93, May 2010.
10. O. Adriani, G. C. Barbarino, G. A. Bazilevskaya, R. Bellotti, M. Boezio, E. A. Bogomolov, L. Bonechi, M. Bongi, V. Bonvicini, S. Borisov, S. Bottai, A. Bruno, F. Cafagna, D. Campana, R. Carbone, P. Carlson, M. Casolino, G. Castellini, L. Consiglio, M. P. De Pascale, C. De Santis, N. De Simone, V. Di Felice, A. M. Galper, W. Gillard, L. Grishantseva, G. Jerse, A. V. Karelin, S. V. Koldashov, S. Y. Krutkov, A. N. Kvashnin, A. Leonov, V. Malakhov, V. Malvezzi, L. Marcelli, A. G. Mayorov, W. Menn, V. V. Mikhailov, E. Mocchiutti, A. Monaco, N. Mori, N. Nikonov,

- G. Osteria, F. Palma, P. Papini, M. Pearce, P. Picozza, C. Pizzolotto, M. Ricci, S. B. Ricciarini, L. Rossetto, R. Sarkar, M. Simon, R. Sparvoli, P. Spillantini, Y. I. Stozhkov, A. Vacchi, E. Vannuccini, G. Vasilyev, S. A. Voronov, Y. T. Yurkin, J. Wu, G. Zampa, N. Zampa, and V. G. Zverev. PAMELA Measurements of Cosmic-Ray Proton and Helium Spectra. *Science*, 332:69, April 2011.
11. M. Aguilar, D. Aisa, B. Alpat, A. Alvino, G. Ambrosi, K. Andeen, L. Arruda, N. Attig, P. Azzarello, A. Bachlechner, F. Barao, A. Barrau, L. Barrin, A. Bartoloni, L. Basara, M. Battarbee, R. Battiston, J. Bazo, U. Becker, M. Behlmann, B. Beischer, J. Berdugo, B. Bertucci, G. Bigongiari, V. Bindi, S. Bizzaglia, M. Bizzarri, G. Boella, W. de Boer, K. Bollweg, V. Bonnivard, B. Borgia, S. Borsini, M. J. Boschini, M. Bourquin, J. Burger, F. Cadoux, X. D. Cai, M. Capell, S. Caroff, J. Casaus, V. Cascioli, G. Castellini, I. Cernuda, D. Cerreta, F. Cervelli, M. J. Chae, Y. H. Chang, A. I. Chen, H. Chen, G. M. Cheng, H. S. Chen, L. Cheng, H. Y. Chou, E. Choumilov, V. Choutko, C. H. Chung, C. Clark, R. Clavero, G. Coignet, C. Consolandi, A. Contin, C. Corti, G. E. Cortina, B. Coste, W. Creus, M. Crispoltoni, Z. Cui, Y. M. Dai, C. Delgado, S. Della Torre, M. B. Demirkoz, L. Derome, S. Di Falco, L. Di Masso, F. Dimiccoli, C. Diaz, P. von Doetinchem, F. Donnini, W. J. Du, M. Duranti, D. D'Urso, A. Eline, F. J. Eppling, T. Eronen, Y. Y. Fan, L. Farnesini, J. Feng, E. Fiandrini, A. Fiasson, E. Finch, P. Fisher, Y. Galaktionov, G. Gallucci, B. Garcia, R. Garcia-Lopez, C. Gargiulo, H. Gast, I. Gebauer, M. Gervasi, A. Ghelfi, W. Gillard, F. Giovacchini, P. Goglov, J. Gong, C. Goy, V. Grabski, D. Grandi, M. Graziani, C. Guandalini, I. Guerri, K. H. Guo, D. Haas, M. Habiby, S. Haino, K. C. Han, Z. H. He, M. Heil, J. Hoffman, T. H. Hsieh, Z. C. Huang, C. Huh, M. Incagli, M. Ionica, W. Y. Jang, H. Jinchi, K. Kanishev, G. N. Kim, K. S. Kim, Th. Kirn, R. Kossakowski, O. Kounina, A. Kounine, V. Koutsenko, M. S. Krafczyk, G. La Vacca, E. Laudi, G. Laurenti, I. Lazzizzera, A. Lebedev, H. T. Lee, S. C. Lee, C. Leluc, G. Levi, H. L. Li, J. Q. Li, Q. Li, Q. Li, T. X. Li, W. Li, Y. Li, Z. H. Li, Z. Y. Li, S. Lim, C. H. Lin, P. Lipari, T. Lippert, D. Liu, H. Liu, M. Lolli, T. Lomtadze, M. J. Lu, S. Q. Lu, Y. S. Lu, K. Luebelsmeyer, J. Z. Luo, S. S. Lv, R. Majka, C. Mana, J. Marin, T. Martin, G. Martinez, N. Masi, D. Maurin, A. Menchaca-Rocha,

- Q. Meng, D. C. Mo, L. Morescalchi, P. Mott, M. Muller, J. Q. Ni, N. Nikonov, F. Nozzoli, P. Nunes, A. Obermeier, A. Oliva, M. Orcinha, F. Palmonari, C. Palomares, M. Paniccia, A. Papi, M. Pauluzzi, E. Pedreschi, S. Pensotti, R. Pereira, N. Picot-Clemente, F. Pilo, A. Piluso, C. Pizzolotto, V. Plyaskin, M. Pohl, V. Poireau, E. Postaci, A. Putze, L. Quadrani, X. M. Qi, X. Qin, Z. Y. Qu, T. Raiha, P. G. Rancoita, D. Rapin, J. S. Ricol, I. Rodriguez, S. Rosier-Lees, A. Rozhkov, D. Rozza, R. Sagdeev, J. Sandweiss, P. Saouter, C. Sbarra, S. Schael, S. M. Schmidt, A. von Dratzig Schulz, G. Schwering, G. Scolieri, E. S. Seo, B. S. Shan, Y. H. Shan, J. Y. Shi, X. Y. Shi, Y. M. Shi, T. Siedenburg, D. Son, F. Spada, F. Spinella, W. Sun, W. H. Sun, M. Tacconi, C. P. Tang, X. W. Tang, Z. C. Tang, L. Tao, D. Tescaro, Samuel C. Ting, S. M. Ting, N. Tomassetti, J. Torsti, C. Turkoglu, T. Urban, V. Vagelli, E. Valente, C. Vannini, E. Valtonen, S. Vaurynovich, M. Vecchi, M. Velasco, J. P. Vialle, V. Vitale, S. Vitillo, L. Q. Wang, N. H. Wang, Q. L. Wang, R. S. Wang, X. Wang, Z. X. Wang, Z. L. Weng, K. Whitman, J. Wienkenhover, H. Wu, X. Wu, X. Xia, M. Xie, S. Xie, R. Q. Xiong, G. M. Xin, N. S. Xu, W. Xu, Q. Yan, J. Yang, M. Yang, Q. H. Ye, H. Yi, Y. J. Yu, Z. Q. Yu, S. Zeissler, J. H. Zhang, M. T. Zhang, X. B. Zhang, Z. Zhang, Z. M. Zheng, H. L. Zhuang, V. Zhukov, A. Zichichi, N. Zimmermann, P. Zucon, C. Zurbach. Precision Measurement of the Proton Flux in Primary Cosmic Rays from Rigidity 1 GV to 1.8 TV with the Alpha Magnetic Spectrometer on the International Space Station. *Phys. Rev. Lett.*, 114(17):171103, May 2015.
12. P. Blasi, E. Amato, and P. D. Serpico. Spectral Breaks as a Signature of Cosmic Ray Induced Turbulence in the Galaxy. *Phys. Rev. Lett.*, 109(6):061101, August 2012.
13. A. E. Vladimirov, G. Jóhannesson, I. V. Moskalenko, and T. A. Porter. Testing the Origin of High-energy Cosmic Rays. *Astrophys. J.*, 752:68, June 2012.
14. V. Ptuskin, V. Zirakashvili, and E.-S. Seo. Spectra of Cosmic-Ray Protons and Helium Produced in Supernova Remnants. *Astrophys. J.*, 763:47, January 2013.

15. Y.-Q. Guo and Q. Yuan. On the knee of Galactic cosmic rays in light of sub-TeV spectral hardenings. *Chinese Physics C*, 42(7):075103, June 2018.
16. Y. S. Yoon, T. Anderson, A. Barrau, N. B. Conklin, S. Coutu, L. Derome, J. H. Han, J. A. Jeon, K. C. Kim, M. H. Kim, H. Y. Lee, J. Lee, M. H. Lee, S. E. Lee, J. T. Link, A. Menchaca-Rocha, J. W. Mitchell, S. I. Mognet, S. Nutter, I. H. Park, N. Picot-Clemente, A. Putze, E. S. Seo, J. Smith, and J. Wu. Proton and Helium Spectra from the CREAM-III Flight. *Astrophys. J.*, 839:5, April 2017.
17. E. Atkin, V. Bulatov, V. Dorokhov, N. Gorbunov, S. Filippov, V. Grebenyuk, D. Karmanov, I. Kovalev, I. Kudryashov, A. Kurganov, M. Merkin, A. Panov, D. Podorozhny, D. Polkov, S. Porokhovoy, V. Shumikhin, A. Tkachenko, L. Tkachev, A. Turundaevskiy, O. Vasiliev, and A. Voronin. New Universal Cosmic-Ray Knee near a Magnetic Rigidity of 10 TV with the NUCLEON Space Observatory. *Soviet Journal of Experimental and Theoretical Physics Letters*, 108:5–12, July 2018.
18. B. Bartoli, P. Bernardini, X. J. Bi, Z. Cao, S. Catalanotti, S. Z. Chen, T. L. Chen, S. W. Cui, B. Z. Dai, A. D’Amone, D. M. Danzengluobu, I., B. D’Ettorre Piazzoli, T. Di Girolamo, G. Di Sciascio, C. F. Feng, Z. Feng, Z. Feng, Q. B. Gou, Y. Q. Guo, H. H. He, H. Hu, H. Hu, M. Iacovacci, R. Iuppa, H. Y. Jia, L. Labaciren, H. J., C. Liu, J. Liu, M. Y. Liu, H. Lu, L. L. Ma, X. H. Ma, G. Mancarella, S. M. Mari, G. Marsella, S. Mastroianni, P. Montini, C. C. Ning, L. Perrone, P. Pistilli, P. Salvini, R. Santonico, G. Settanta, P. R. Shen, X. D. Sheng, F. Shi, A. Surdo, Y. H. Tan, P. Vallania, S. Vernetto, C. Vigorito, H. Wang, C. Y. Wu, H. R. Wu, L. Xue, Q. Y. Yang, X. C. Yang, Z. G. Yao, A. F. Yuan, M. Zha, H. M. Zhang, L. Zhang, X. Y. Zhang, Y. Zhang, J. Zhao, X. X. Z. Zhaxiciren, Zhou, F. R. Zhu, Q. Q. Zhu, and ARGO-YBJ Collaboration. Cosmic ray proton plus helium energy spectrum measured by the ARGO-YBJ experiment in the energy range 3-300 TeV. *Phys. Rev. D*, 91(11):112017, June 2015.

19. J. Chang, Dark Matter Particle Explorer: The First Chinese Cosmic Ray and Hard Gamma-ray Detector in Space. *Chin. J. Space Sci.*, **34**, 550 (2014).
20. J. Chang, G. Ambrosi, Q. An, R. Asfandiyarov, P. Azzarello, P. Bernardini, B. Bertucci, M. S. Cai, M. Caragiulo, D. Y. Chen, H. F. Chen, J. L. Chen, W. Chen, M. Y. Cui, T. S. Cui, A. D’Amone, A. De Benedittis, I. De Mitri, M. Di Santo, J. N. Dong, T. K. Dong, Y. F. Dong, Z. X. Dong, G. Donvito, D. Droz, K. K. Duan, J. L. Duan, M. Duranti, D. D’Urso, R. R. Fan, Y. Z. Fan, F. Fang, C. Q. Feng, L. Feng, P. Fusco, V. Gallo, F. J. Gan, W. Q. Gan, M. Gao, S. S. Gao, F. Gargano, K. Gong, Y. Z. Gong, J. H. Guo, Y. M. Hu, G. S. Huang, Y. Y. Huang, M. Ionica, D. Jiang, W. Jiang, X. Jin, J. Kong, S. J. Lei, S. Li, X. Li, W. L. Li, Y. Li, Y. F. Liang, Y. M. Liang, N. H. Liao, Q. Z. Liu, H. Liu, J. Liu, S. B. Liu, Q. Z. Liu, W. Q. Liu, Y. Liu, F. Loparco, J. Lü, M. Ma, P. X. Ma, S. Y. Ma, T. Ma, X. Q. Ma, X. Y. Ma, G. Marsella, M. N. Mazziotta, D. Mo, T. T. Miao, X. Y. Niu, M. Pohl, X. Y. Peng, W. X. Peng, R. Qiao, J. N. Rao, M. M. Salinas, G. Z. Shang, W. H. Shen, Z. Q. Shen, Z. T. Shen, J. X. Song, H. Su, M. Su, Z. Y. Sun, A. Surdo, X. J. Teng, X. B. Tian, A. Tykhonov, V. Vagelli, S. Vitillo, C. Wang, C. Wang, H. Wang, H. Y. Wang, J. Z. Wang, L. G. Wang, Q. Wang, S. Wang, X. H. Wang, X. L. Wang, Y. F. Wang, Y. P. Wang, Y. Z. Wang, S. C. Wen, Z. M. Wang, D. M. Wei, J. J. Wei, Y. F. Wei, D. Wu, J. Wu, S. S. Wu, X. Wu, K. Xi, Z. Q. Xia, Y. L. Xin, H. T. Xu, Z. L. Xu, Z. Z. Xu, G. F. Xue, H. B. Yang, J. Yang, P. Yang, Y. Q. Yang, Z. L. Yang, H. J. Yao, Y. H. Yu, Q. Yuan, C. Yue, J. J. Zang, C. Zhang, D. L. Zhang, F. Zhang, J. B. Zhang, J. Y. Zhang, J. Z. Zhang, L. Zhang, P. F. Zhang, S. X. Zhang, W. Z. Zhang, Y. Zhang, Y. J. Zhang, Y. Q. Zhang, Y. L. Zhang, Y. P. Zhang, Z. Zhang, Z. Y. Zhang, H. Zhao, H. Y. Zhao, X. F. Zhao, C. Y. Zhou, Y. Zhou, X. Zhu, Y. Zhu, and S. Zimmer. The DARK Matter Particle Explorer mission. *Astroparticle Physics*, 95:6–24, October 2017.
21. Y. Yu, Z. Sun, H. Su, Y. Yang, J. Liu, J. Kong, G. Xiao, X. Ma, Y. Zhou, H. Zhao, D. Mo, Y. Zhang, P. Yang, J. Chen, H. Yang, F. Fang, S. Zhang, H. Yao, J. Duan, X. Niu, Z. Hu, Z. Wang, X. Wang,

- J. Zhang, and W. Liu. The plastic scintillator detector for DAMPE. *Astroparticle Physics*, 94:1–10, September 2017.
22. P. Azzarello, G. Ambrosi, R. Asfandiyarov, P. Bernardini, B. Bertucci, A. Bolognini, F. Cadoux, M. Caprai, I. De Mitri, M. Domenjuz, Y. Dong, M. Duranti, R. Fan, P. Fusco, V. Gallo, F. Gargano, K. Gong, D. Guo, C. Husi, M. Ionica, D. La Marra, F. Loparco, G. Marsella, M. N. Mazziotta, J. Mesa, A. Nardinocchi, L. Nicola, G. Pelleriti, W. Peng, M. Pohl, V. Postolache, R. Qiao, A. Surdo, A. Tykhonov, S. Vitillo, H. Wang, M. Weber, D. Wu, X. Wu, and F. Zhang. The DAMPE silicon-tungsten tracker. *Nuclear Instruments and Methods in Physics Research A*, 831:378–384, September 2016.
23. Z. Zhang, Y. Zhang, J. Dong, S. Wen, C. Feng, C. Wang, Y. Wei, X. Wang, Z. Xu, and S. Liu. Design of a high dynamic range photomultiplier base board for the BGO ECAL of DAMPE. *Nuclear Instruments and Methods in Physics Research A*, 780:21–26, April 2015.
24. M. He, T. Ma, J. Chang, Y. Zhang, Y. Y. Huang, J. J. Zang, J. Wu, and T. K. Dong. GEANT4 Simulation of Neutron Detector for DAMPE. *Acta Astronomica Sinica*, 57:1–8, January 2016.
25. T.-K. Dong, Y.-P. Zhang, P.-X. Ma, Y.-J. Zhang, P. Bernardini, M. Ding, D.-Y. Guo, S.-J. Lei, X. Li, I. De Mitri, W.-X. Peng, R. Qiao, M. Di Santo, Z.-Y. Sun, A. Surdo, Z.-M. Wang, J. Wu, Z.-L. Xu, Y.-H. Yu, Q. Yuan, C. Yue, J.-J. Zang, Y.-L. Zhang. Charge measurement of cosmic ray nuclei with the plastic scintillator detector of DAMPE. *Astropart. Phys.*, 105:31–36, 2019.
26. DAMPE Collaboration, G. Ambrosi, Q. An, R. Asfandiyarov, P. Azzarello, P. Bernardini, B. Bertucci, M. S. Cai, J. Chang, D. Y. Chen, H. F. Chen, J. L. Chen, W. Chen, M. Y. Cui, T. S. Cui, A. D’Amone, A. de Benedittis, I. De Mitri, M. di Santo, J. N. Dong, T. K. Dong, Y. F. Dong, Z. X. Dong, G. Donvito, D. Droz, K. K. Duan, J. L. Duan, M. Duranti, D. D’Urso, R. R. Fan, Y. Z. Fan, F. Fang, C. Q. Feng, L. Feng, P. Fusco, V. Gallo, F. J. Gan, M. Gao, S. S. Gao, F. Gargano,

S. Garrappa, K. Gong, Y. Z. Gong, D. Y. Guo, J. H. Guo, Y. M. Hu, G. S. Huang, Y. Y. Huang, M. Ionica, D. Jiang, W. Jiang, X. Jin, J. Kong, S. J. Lei, S. Li, X. Li, W. L. Li, Y. Li, Y. F. Liang, Y. M. Liang, N. H. Liao, H. Liu, J. Liu, S. B. Liu, W. Q. Liu, Y. Liu, F. Loparco, M. Ma, P. X. Ma, S. Y. Ma, T. Ma, X. Q. Ma, X. Y. Ma, G. Marsella, M. N. Mazziotta, D. Mo, X. Y. Niu, X. Y. Peng, W. X. Peng, R. Qiao, J. N. Rao, M. M. Salinas, G. Z. Shang, W. H. Shen, Z. Q. Shen, Z. T. Shen, J. X. Song, H. Su, M. Su, Z. Y. Sun, A. Surdo, X. J. Teng, X. B. Tian, A. Tykhonov, V. Vagelli, S. Vitillo, C. Wang, H. Wang, H. Y. Wang, J. Z. Wang, L. G. Wang, Q. Wang, S. Wang, X. H. Wang, X. L. Wang, Y. F. Wang, Y. P. Wang, Y. Z. Wang, S. C. Wen, Z. M. Wang, D. M. Wei, J. J. Wei, Y. F. Wei, D. Wu, J. Wu, L. B. Wu, S. S. Wu, X. Wu, K. Xi, Z. Q. Xia, Y. L. Xin, H. T. Xu, Z. L. Xu, Z. Z. Xu, G. F. Xue, H. B. Yang, P. Yang, Y. Q. Yang, Z. L. Yang, H. J. Yao, Y. H. Yu, Q. Yuan, C. Yue, J. J. Zang, C. Zhang, D. L. Zhang, F. Zhang, J. B. Zhang, J. Y. Zhang, J. Z. Zhang, L. Zhang, P. F. Zhang, S. X. Zhang, W. Z. Zhang, Y. Zhang, Y. J. Zhang, Y. Q. Zhang, Y. L. Zhang, Y. P. Zhang, Z. Zhang, Z. Y. Zhang, H. Zhao, H. Y. Zhao, X. F. Zhao, C. Y. Zhou, Y. Zhou, X. Zhu, Y. Zhu, and S. Zimmer. Direct detection of a break in the teraelectronvolt cosmic-ray spectrum of electrons and positrons. *Nature*, 552:63–66, December 2017.

27. G. Ambrosi, Q. An, R. Asfandiyarov, P. Azzarello, P. Bernardini, M. S. Cai, M. Caragiulo, J. Chang, D. Y. Chen, H. F. Chen, J. L. Chen, W. Chen, M. Y. Cui, T. S. Cui, H. T. Dai, A. D’Amone, A. De Benedittis, I. De Mitri, M. Ding, M. Di Santo, J. N. Dong, T. K. Dong, Y. F. Dong, Z. X. Dong, D. Droz, K. K. Duan, J. L. Duan, D. D’Urso, R. R. Fan, Y. Z. Fan, F. Fang, C. Q. Feng, L. Feng, P. Fusco, V. Gallo, F. J. Gan, M. Gao, S. S. Gao, F. Gargano, S. Garrappa, K. Gong, Y. Z. Gong, J. H. Guo, Y. M. Hu, G. S. Huang, Y. Y. Huang, M. Ionica, D. Jiang, W. Jiang, X. Jin, J. Kong, S. J. Lei, S. Li, X. Li, W. L. Li, Y. Li, Y. F. Liang, Y. M. Liang, N. H. Liao, C. M. Liu, H. Liu, J. Liu, S. B. Liu, W. Q. Liu, Y. Liu, F. Loparco, M. Ma, P. X. Ma, S. Y. Ma, T. Ma, X. Q. Ma, X. Y. Ma, G. Marsella, M. N. Mazziotta, D. Mo, X. Y. Niu, X. Pan, X. Y. Peng, W. X. Peng, R. Qiao, J. N. Rao, M. M. Salinas, G. Z. Shang, W. H. Shen, Z. Q. Shen, Z. T. Shen, J. X. Song, H.

Su, M. Su, Z. Y. Sun, A. Surdo, X. J. Teng, X. B. Tian, A. Tykhonov, S. Vitillo, C. Wang, H. Wang, H. Y. Wang, J. Z. Wang, L. G. Wang, Q. Wang, S. Wang, X. H. Wang, X. L. Wang, Y. F. Wang, Y. P. Wang, Y. Z. Wang, Z. M. Wang, S. C. Wen, D. M. Wei, J. J. Wei, Y. F. Wei, D. Wu, J. Wu, L. B. Wu, S. S. Wu, X. Wu, K. Xi, Z. Q. Xia, Y. L. Xin, H. T. Xu, Z. H. Xu, Z. L. Xu, Z. Z. Xu, G. F. Xue, H. B. Yang, P. Yang, Y. Q. Yang, Z. L. Yang, H. J. Yao, Y. H. Yu, Q. Yuan, C. Yue, J. J. Zang, D. L. Zhang, F. Zhang, J. B. Zhang, J. Y. Zhang, J. Z. Zhang, L. Zhang, P. F. Zhang, S. X. Zhang, W. Z. Zhang, Y. Zhang, Y. J. Zhang, Y. Q. Zhang, Y. L. Zhang, Y. P. Zhang, Z. Zhang, Z. Y. Zhang, H. Zhao, H. Y. Zhao, X. F. Zhao, C. Y. Zhou, Y. Zhou, X. Zhu, Y. Zhu, and S. Zimmer. The on-orbit calibration of DArk Matter Particle Explorer. *Astropart. Phys.*, 106:18–34, 2019.

28. S. Agostinelli, J. Allison, K. Amako, J. Apostolakis, H. Araujo, P. Arce, M. Asai, D. Axen, S. Banerjee, G. Barrand, F. Behner, L. Bellagamba, J. Boudreau, L. Broglia, A. Brunengo, H. Burkhardt, S. Chauvie, J. Chuma, R. Chytrcek, G. Cooperman, G. Cosmo, P. Degtyarenko, A. Dell’Acqua, G. Depaola, D. Dietrich, R. Enami, A. Feliciello, C. Ferguson, H. Fesefeldt, G. Folger, F. Foppiano, A. Forti, S. Garelli, S. Giani, R. Giannitrapani, D. Gibin, J. J. Gómez Cadenas, I. González, G. Gracia Abril, G. Greeniaus, W. Greiner, V. Grichine, A. Grossheim, S. Guatelli, P. Gumplinger, R. Hamatsu, K. Hashimoto, H. Hasui, A. Heikkinen, A. Howard, V. Ivanchenko, A. Johnson, F. W. Jones, J. Kallenbach, N. Kanaya, M. Kawabata, Y. Kawabata, M. Kawaguti, S. Kelner, P. Kent, A. Kimura, T. Kodama, R. Kokoulin, M. Kossov, H. Kurashige, E. Lamanna, T. Lampén, V. Lara, V. Lefebure, F. Lei, M. Liendl, W. Lockman, F. Longo, S. Magni, M. Maire, E. Medernach, K. Minamimoto, P. Mora de Freitas, Y. Morita, K. Murakami, M. Nagamatu, R. Nartallo, P. Nieminen, T. Nishimura, K. Ohtsubo, M. Okamura, S. O’Neale, Y. Oohata, K. Paech, J. Perl, A. Pfeiffer, M. G. Pia, F. Ranjard, A. Rybin, S. Sadilov, E. Di Salvo, G. Santin, T. Sasaki, N. Savvas, Y. Sawada, S. Scherer, S. Sei, V. Sirotenko, D. Smith, N. Starkov, H. Stoecker, J. Sulkimo, M. Takahata, S. Tanaka, E. Tcherniaev, E. Safai Tehrani, M. Tropeano, P. Truscott, H. Uno, L. Urban, P. Urban, M. Verderi, A. Walkden, W. Wander, H. Weber, J. P. Wellisch, T. We-

- naus, D. C. Williams, D. Wright, T. Yamada, H. Yoshida, D. Zschesche, and GEANT4 Collaboration. GEANT4—a simulation toolkit. *Nuclear Instruments and Methods in Physics Research A*, 506:250–303, July 2003.
29. R. Aloisio, P. Blasi, I. De Mitri, and S. Petrer. *Selected Topics in Cosmic Ray Physics*, 2018.
30. B. Bartoli, P. Bernardini, X. J. Bi, Z. Cao, S. Catalanotti, S. Z. Chen, T. L. Chen, S. W. Cui, B. Z. Dai, A. D’Amone, Danzengluobu, I. De Mitri, B. D’Ettorre Piazzoli, T. Di Girolamo, G. Di Sciascio, C. F. Feng, Z. Feng, Z. Feng, W. Gao, Q. B. Gou, Y. Q. Guo, H. H. He, H. Hu, H. Hu, M. Iacovacci, R. Iuppa, H. Y. Jia, Labaciren, H. J. Li, C. Liu, J. Liu, M. Y. Liu, H. Lu, L. L. Ma, X. H. Ma, G. Mancarella, S. M. Mari, G. Marsella, S. Mastroianni, P. Montini, C. C. Ning, L. Perrone, P. Pistilli, P. Salvini, R. Santonico, P. R. Shen, X. D. Sheng, F. Shi, A. Surdo, Y. H. Tan, P. Vallania, S. Vernetto, C. Vigorito, H. Wang, C. Y. Wu, H. R. Wu, L. Xue, Q. Y. Yang, X. C. Yang, Z. G. Yao, A. F. Yuan, M. Zha, H. M. Zhang, L. Zhang, X. Y. Zhang, Y. Zhang, J. Zhao, Zhaxiciren, Zhaxisangzhu, X. X. Zhou, F. R. Zhu, Q. Q. Zhu, and ARGO-YBJ Collaboration. ARGO-YBJ Observation of the Large-scale Cosmic Ray Anisotropy During the Solar Minimum between Cycles 23 and 24. *Astrophys. J.*, 809:90, August 2015.
31. W. Liu, X.-J. Bi, S.-J. Lin, B.-B. Wang, and P.-F. Yin. Excesses of cosmic ray spectra from a single nearby source. *Phys. Rev. D*, 96(2):023006, July 2017.
32. V. I. Zatsepin and N. V. Sokolskaya. Three component model of cosmic ray spectra from 10 GeV to 100 PeV. *Astron. Astrophys*, 458:1–5, October 2006.
33. T. T. Böhlen, F. Cerutti, M. P. W. Chin, A. Fassò, A. Ferrari, P. G. Ortega, A. Mairani, P. R. Sala, G. Smirnov, and V. Vlachoudis. The FLUKA Code: Developments and Challenges for High Energy and Medical Applications. *Nuclear Data Sheets*, 120:211–214, June 2014.

34. P.-X. Ma, Y.-J. Zhang, Y.-P. Zhang, Y. Li, J.-J. Zang, X. Li, T.-K. Dong, Y.-Z. Fan, S.-J. Lei, J. Wu, Y.-H. Yu, Q. Yuan, C. Yue, and Z.-Y. Sun. A Method of Alignment of the Plastic Scintillator Detector of DAMPE. *Res. Astron. Astrophys.* 19(6):82, June 2019.
35. A. Tykhonov, G. Ambrosi, R. Asfandiyarov, P. Azzarello, P. Bernardini, B. Bertucci, A. Bolognini, F. Cadoux, A. D'Amone, A. De Benedittis, I. De Mitri, M. Di Santo, Y. F. Dong, M. Duranti, D. D'Urso, R. R. Fan, P. Fusco, V. Gallo, M. Gao, F. Gargano, S. Garrappa, K. Gong, M. Ionica, D. La Marra, S. J. Lei, X. Li, F. Loparco, G. Marsella, M. N. Mazziotta, W. X. Peng, R. Qiao, M. M. Salinas, A. Surdo, V. Vagelli, S. Vitillo, H. Y. Wang, J. Z. Wang, Z. M. Wang, D. Wu, X. Wu, F. Zhang, J. Y. Zhang, H. Zhao, and S. Zimmer. Internal alignment and position resolution of the silicon tracker of DAMPE determined with orbit data. *Nuclear Instruments and Methods in Physics Research A*, 893:43–56, June 2018.
36. Z. Zhang, C. Wang, J. Dong, Y. Wei, S. Wen, Y. Zhang, Z. Li, C. Feng, S. Gao, Z. Shen, D. Zhang, J. Zhang, Q. Wang, S. Ma, D. Yang, D. Jiang, D. Chen, Y. Hu, G. Huang, X. Wang, Z. Xu, S. Liu, Q. An, and Y. Gong. The calibration and electron energy reconstruction of the BGO ECAL of the DAMPE detector. *Nuclear Instruments and Methods in Physics Research A*, 836:98–104, November 2016.
37. C. Yue, J. Zang, T. Dong, X. Li, Z. Zhang, S. Zimmer, W. Jiang, Y. Zhang, and D. Wei. A parameterized energy correction method for electromagnetic showers in BGO-ECAL of DAMPE. *Nuclear Instruments and Methods in Physics Research A*, 856:11–16, June 2017.
38. G. D'Agostini. A multidimensional unfolding method based on Bayes' theorem. *Nuclear Instruments and Methods in Physics Research A*, 362:487–498, February 1995.
39. CRMC (Cosmic Ray Monte Carlo package), <https://web.ikp.kit.edu/rulrich/crmc.html>

40. J. J. Zang, C. Yue, and X. Li. Measurement of absolute energy scale of ECAL of DAMPE with geomagnetic rigidity cutoff. *PoS, ICRC2017:197*, 2018; <https://pos.sissa.it/301/197/pdf>.
41. S. Abdollahi, M. Ackermann, M. Ajello, W. B. Atwood, L. Baldini, G. Barbiellini, D. Bastieri, R. Bellazzini, E. D. Bloom, R. Bonino, T. J. Brandt, J. Bregeon, P. Bruel, R. Buehler, R. A. Cameron, R. Caputo, M. Caragiulo, D. Castro, E. Cavazzuti, C. Cecchi, A. Chekhtman, S. Ciprini, J. Cohen-Tanugi, F. Costanza, A. Cuoco, S. Cutini, F. D'Ammando, F. de Palma, R. Desiante, S. W. Digel, N. Di Lalla, M. Di Mauro, L. Di Venere, P. S. Drell, A. Drlica-Wagner, C. Favuzzi, W. B. Focke, S. Funk, P. Fusco, F. Gargano, D. Gasparrini, N. Giglietto, F. Giordano, M. Giroletti, D. Green, L. Guillemot, S. Guiriec, A. K. Harding, T. Jogler, G. Jóhannesson, T. Kamae, M. Kuss, G. La Mura, L. Latronico, F. Longo, F. Loparco, P. Lubrano, S. Maldera, D. Malyshev, A. Manfreda, M. N. Mazziotta, P. F. Michelson, N. Mirabal, W. Mitthumsiri, T. Mizuno, A. A. Moiseev, M. E. Monzani, A. Morselli, I. V. Moskalenko, M. Negro, E. Nuss, E. Orlando, D. Paneque, J. S. Perkins, M. Pesce-Rollins, F. Piron, G. Pivato, T. A. Porter, G. Principe, S. Rainò, R. Rando, M. Razzano, A. Reimer, O. Reimer, C. Sgrò, D. Simone, E. J. Siskind, F. Spada, G. Spandre, P. Spinelli, H. Tajima, J. B. Thayer, L. Tibaldo, D. F. Torres, E. Troja, M. Wood, A. Worley, G. Zaharijas, S. Zimmer, and Fermi-LAT Collaboration. Cosmic-ray electron-positron spectrum from 7 GeV to 2 TeV with the Fermi Large Area Telescope. *Phys. Rev. D*, 95(8):082007, April 2017.
42. O. Adriani, Y. Akaike, K. Asano, Y. Asaoka, M. G. Bagliesi, E. Berti, G. Bigongiari, W. R. Binns, S. Bonechi, M. Bongi, P. Brogi, A. Bruno, J. H. Buckley, N. Cannady, G. Castellini, C. Checchia, M. L. Cherry, G. Collazuol, V. di Felice, K. Ebisawa, H. Fuke, T. G. Guzik, T. Hams, N. Hasebe, K. Hibino, M. Ichimura, K. Ioka, W. Ishizaki, M. H. Israel, K. Kasahara, J. Kataoka, R. Kataoka, Y. Katayose, C. Kato, N. Kawanaka, Y. Kawakubo, K. Kohri, H. S. Krawczynski, J. F. Krizmanic, T. Lomtadze, P. Maestro, P. S. Marrocchesi, A. M. Messineo, J. W. Mitchell, S. Miyake, A. A. Moiseev, K. Mori, M. Mori, N. Mori, H. M. Motz, K. Munakata, H. Murakami, S. Nakahira, J.

- Nishimura, G. A. de Nolfo, S. Okuno, J. F. Ormes, S. Ozawa, L. Pacini, F. Palma, P. Papini, A. V. Penacchioni, B. F. Rauch, S. B. Ricciarini, K. Sakai, T. Sakamoto, M. Sasaki, Y. Shimizu, A. Shiomi, R. Sparvoli, P. Spillantini, F. Stolzi, J. E. Suh, A. Sulaj, I. Takahashi, M. Takayanagi, M. Takita, T. Tamura, T. Terasawa, H. Tomida, S. Torii, Y. Tsunesada, Y. Uchihori, S. Ueno, E. Vannuccini, J. P. Wefel, K. Yamaoka, S. Yanagita, A. Yoshida, K. Yoshida, and CALET Collaboration. Direct Measurement of the Cosmic-Ray Proton Spectrum from 50 GeV to 10 TeV with the Calorimetric Electron Telescope on the International Space Station. *Phys. Rev. Lett.*, 122(18):181102, May 2019.
43. O. Adriani, G. C. Barbarino, G. A. Bazilevskaya, R. Bellotti, M. Boezio, E. A. Bogomolov, M. Bongi, V. Bonvicini, S. Bottai, A. Bruno, F. Cafagna, D. Campana, R. Carbone, P. Carlson, M. Casolino, G. Castellini, M. P. De Pascale, C. De Santis, N. De Simone, V. Di Felice, V. Formato, A. M. Galper, U. Giaccari, A. V. Karelin, M. D. Kheymits, S. V. Koldashov, S. Koldobskiy, S. Y. Krut'kov, A. N. Kvashnin, A. Leonov, V. Malakhov, L. Marcelli, M. Martucci, A. G. Mayorov, W. Menn, V. V. Mikhailov, E. Mocchiutti, A. Monaco, N. Mori, R. Munini, N. Nikonov, G. Osteria, P. Papini, M. Pearce, P. Picozza, C. Pizzolotto, M. Ricci, S. B. Ricciarini, L. Rossetto, R. Sarkar, M. Simon, R. Sparvoli, P. Spillantini, Y. I. Stozhkov, A. Vacchi, E. Vannuccini, G. I. Vasilyev, S. A. Voronov, J. Wu, Y. T. Yurkin, G. Zampa, N. Zampa, and V. G. Zverev. The PAMELA Mission: Heralding a new era in precision cosmic ray physics. *Phys. Rep.*, 544:323–370, November 2014.
44. O. Adriani, G. C. Barbarino, G. A. Bazilevskaya, R. Bellotti, M. Boezio, E. A. Bogomolov, M. Bongi, V. Bonvicini, S. Bottai, A. Bruno, F. Cafagna, D. Campana, P. Carlson, M. Casolino, G. Castellini, C. De Santis, V. Di Felice, A. M. Galper, A. V. Karelin, S. V. Koldashov, S. Koldobskiy, S. Y. Krutkov, A. N. Kvashnin, A. Leonov, V. Malakhov, L. Marcelli, M. Martucci, A. G. Mayorov, W. Menn, M. Mergegrave, V. V. Mikhailov, E. Mocchiutti, A. Monaco, R. Munini, N. Mori, G.

Osteria, B. Panico, P. Papini, M. Pearce, P. Picozza, M. Ricci, S. B. Ricciarini, M. Simon, R. Sparvoli, P. Spillantini, Y. I. Stozhkov, A. Vacchi, E. Vannuccini, G. Vasilyev, S. A. Voronov, Y. T. Yurkin, G. Zampa, and N. Zampa. Ten years of PAMELA in space. *Riv. Nuovo Cim.*, 40(10):1, 2017.

Acknowledgements

The DAMPE mission is funded by the strategic priority science and technology projects in space science of Chinese Academy of Sciences.

Funding

In China the data analysis was supported in part by the National Key Research and Development Program of China (No. 2016YFA0400200), the National Natural Science Foundation of China (Nos. 11525313, 11622327, 11722328, U1738205, U1738207, U1738208), the strategic priority science and technology projects of Chinese Academy of Sciences (No. XDA15051100), the 100 Talents Program of Chinese Academy of Sciences, and the Young Elite Scientists Sponsorship Program. In Europe the activities and the data analysis are supported by the Swiss National Science Foundation (SNSF), Switzerland; the National Institute for Nuclear Physics (INFN), Italy.

Author contributions

This work is the result of the contributions and efforts of all the participating institutes. All authors have reviewed, discussed, and commented on the results and on the manuscript. In line with the collaboration policy, the authors are listed here alphabetically.

Competing interests

The authors declare no competing interests.

Data and materials availability

The cosmic ray proton fluxes along with statistical and systematics uncertainties are available in Table 1.

Additional requests can be addressed to the DAMPE Collaboration (dampe@pmo.ac.cn).

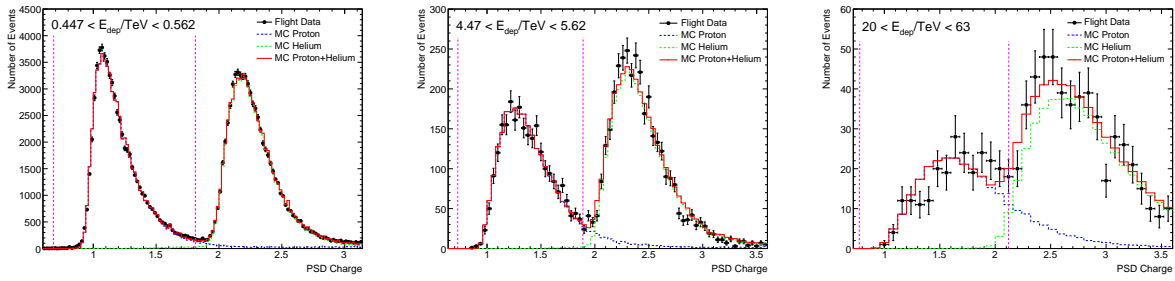


Figure 1: **The combined signal spectra of PSD for protons and helium nuclei.** The left panel is for BGO deposited energies between 447 GeV and 562 GeV, the middle panel is for BGO deposited energies of 4.47 – 5.62 TeV, and the right panel is for BGO deposited energies between 20 TeV and 63 TeV. The on-orbit data (black) are shown, together with the best-fit templates of simulations of protons (blue), helium nuclei (green), and their sum (red). The vertical dashed lines show the cuts to select proton candidates in this deposited energy range.

Table 1. **Fluxes of CR protons measured with DAMPE, together with 1σ statistical and systematic uncertainties.** The systematic uncertainties include those associated with the analysis procedure σ_{ana} (e.g., the event selection, the background subtraction, and the spectral deconvolution), and the energy responses due to different hadronic models σ_{had} .

$\langle E \rangle$ (GeV)	E_{min} (GeV)	E_{max} (GeV)	$F \pm \sigma_{\text{stat}} \pm \sigma_{\text{ana}} \pm \sigma_{\text{had}}$ ($\text{GeV}^{-1}\text{m}^{-2}\text{s}^{-1}\text{sr}^{-1}$)
49.8	39.8	63.1	$(2.97 \pm 0.00 \pm 0.14 \pm 0.20) \times 10^{-1}$
78.9	63.1	100.0	$(8.43 \pm 0.00 \pm 0.40 \pm 0.56) \times 10^{-2}$
125.1	100.0	158.5	$(2.38 \pm 0.00 \pm 0.11 \pm 0.16) \times 10^{-2}$
198.3	158.5	251.2	$(6.64 \pm 0.00 \pm 0.31 \pm 0.44) \times 10^{-3}$
314.3	251.2	398.1	$(1.89 \pm 0.00 \pm 0.09 \pm 0.12) \times 10^{-3}$
498.1	398.1	631.0	$(5.39 \pm 0.01 \pm 0.25 \pm 0.36) \times 10^{-4}$
789.5	631.0	1000	$(1.60 \pm 0.00 \pm 0.07 \pm 0.11) \times 10^{-4}$
1251	1000	1585	$(4.81 \pm 0.01 \pm 0.23 \pm 0.33) \times 10^{-5}$
1983	1585	2512	$(1.45 \pm 0.01 \pm 0.07 \pm 0.13) \times 10^{-5}$
3143	2512	3981	$(4.45 \pm 0.02 \pm 0.21 \pm 0.44) \times 10^{-6}$
4981	3981	6310	$(1.36 \pm 0.01 \pm 0.06 \pm 0.13) \times 10^{-6}$
7895	6310	10000	$(4.06 \pm 0.04 \pm 0.19 \pm 0.40) \times 10^{-7}$
12512	10000	15849	$(1.20 \pm 0.02 \pm 0.06 \pm 0.12) \times 10^{-7}$
19830	15849	25119	$(3.35 \pm 0.07 \pm 0.17 \pm 0.33) \times 10^{-8}$
31429	25119	39811	$(9.03 \pm 0.26 \pm 0.48 \pm 0.89) \times 10^{-9}$
49812	39811	63096	$(2.47 \pm 0.11 \pm 0.15 \pm 0.24) \times 10^{-9}$
78946	63096	100000	$(6.50 \pm 0.40 \pm 0.50 \pm 0.64) \times 10^{-10}$

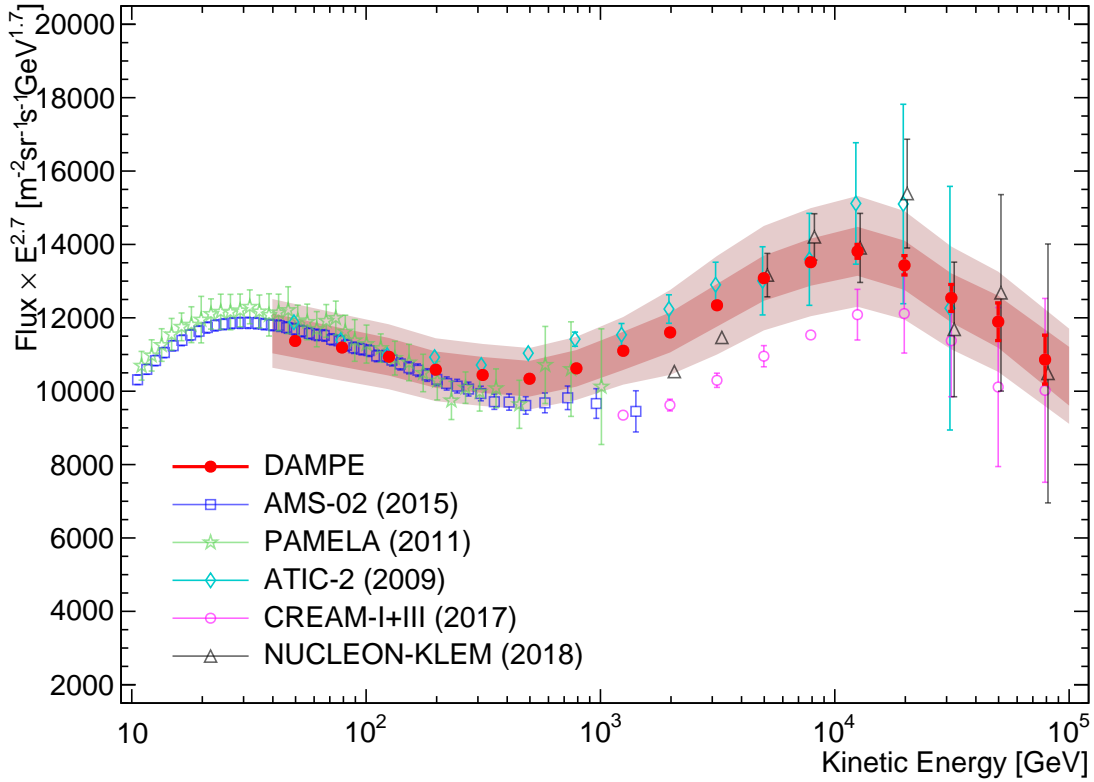


Figure 2: **Proton spectrum from 40 GeV to 100 TeV measured with DAMPE (red filled dots)**. The red error bars show the statistical uncertainties, the inner shaded band shows the estimated systematic uncertainties due to the analysis procedure, and the outer band shows the total systematic uncertainties including also those from the hadronic models. The other direct measurements by PAMELA (10) (green stars), AMS-02 (11) (blue squares), ATIC-2 (7) (cyan diamonds), CREAM I+III (16) (magenta circles), and NUCLEON KLEM (17) are shown for comparison. For the PAMELA data, a -3.2% correction of the absolute fluxes has been included (43, 44). The error bars of PAMELA and AMS-02 data include both statistical and systematic uncertainties added in quadrature. For ATIC, CREAM, and NUCLEON data only statistical uncertainties are shown.

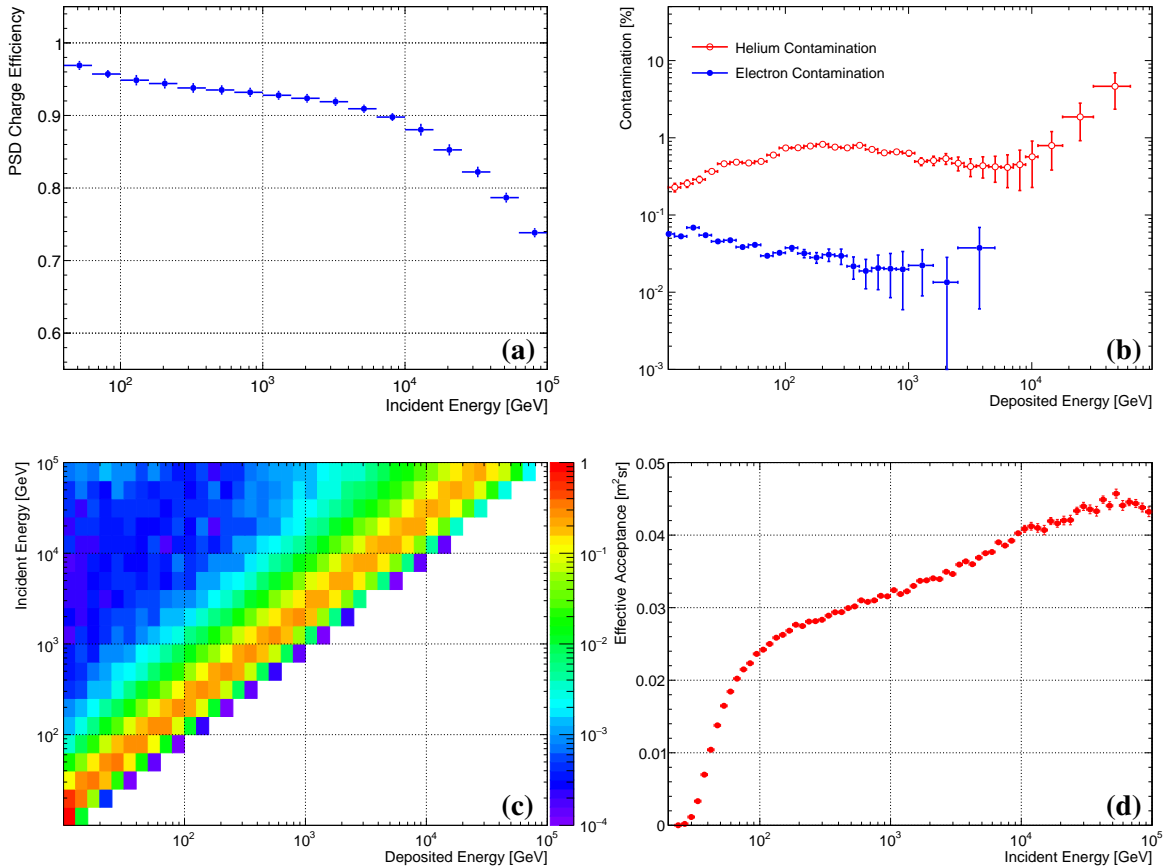


Figure 3: **Some key information for the proton spectrum measurement.** (a) The charge selection efficiency of protons versus incident energies for the GEANT FTFP_BERT model. (b) The fraction of helium (red open circles) and electron (blue filled dots) backgrounds in the proton candidate events as a function of deposited energy. (c) Probability distribution of deposited energies in the BGO calorimeter for different incident energies, for the GEANT FTFP_BERT model. The color represents the fraction of events in each energy bin. (d) Effective acceptance of protons versus incident energies for the GEANT FTFP_BERT model.

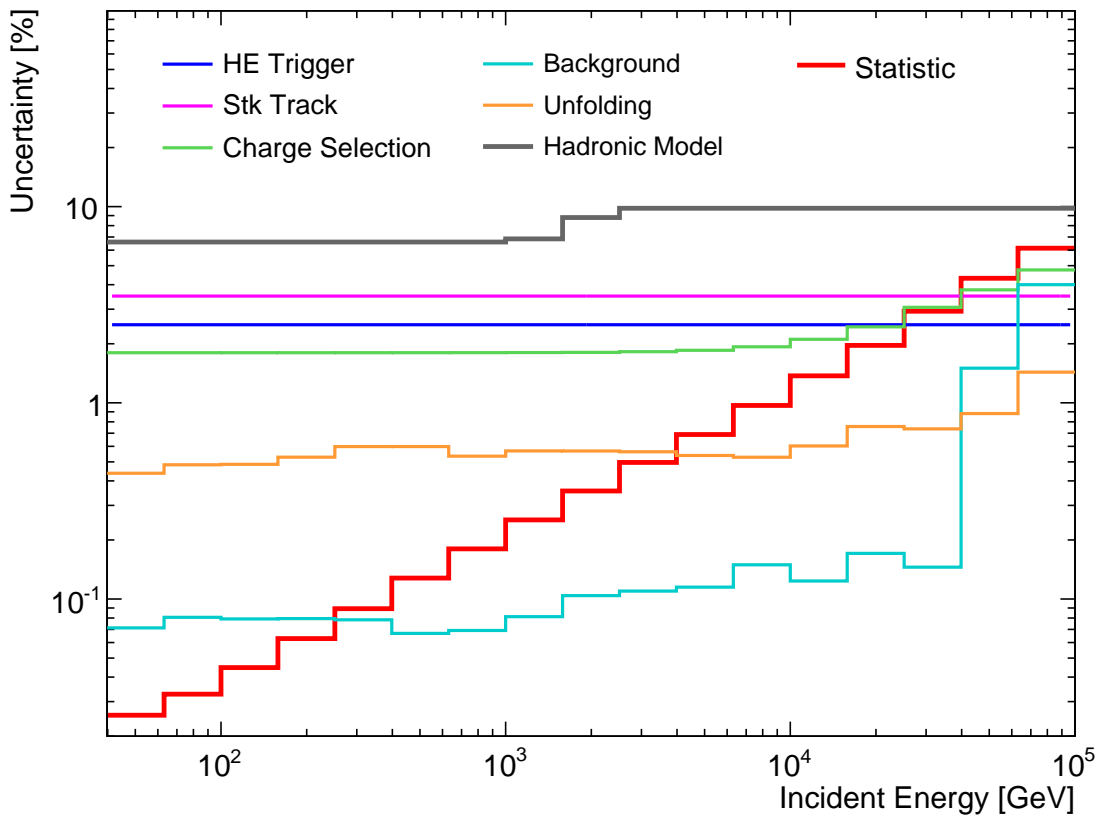


Figure 4: **Statistical and systematic uncertainties of the proton flux measurements.**

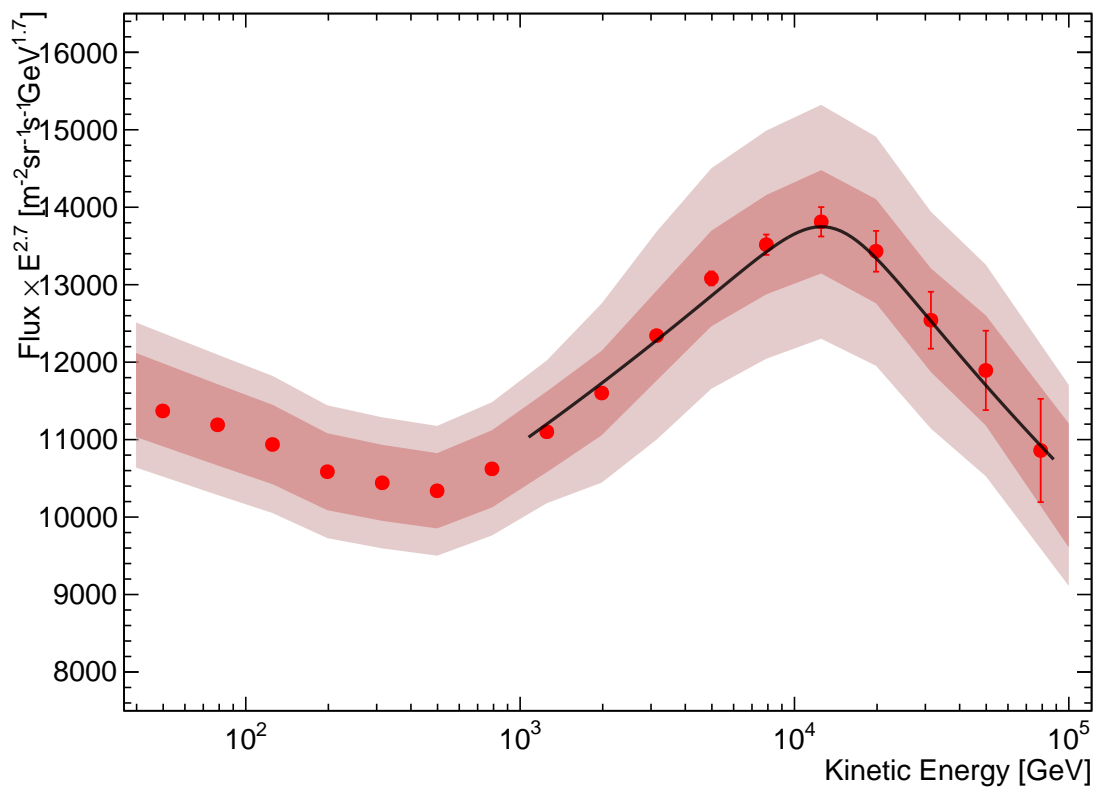


Figure 5: Comparison between the best-fitting of the proton spectrum from 1 TeV to 100 TeV with the smoothly broken power-law function (solid line) and the DAMPE data.